Large-Scale Dune Aurora Event Investigation Combining Citizen Scientists' Photographs and Spacecraft Observations

Grandin, Maxime

2021-06

Grandin , M , Palmroth , M , Whipps , G , Kalliokoski , M , Ferrier , M , Paxton , L J , Mlynczak , M G , Hilska , J , Holmseth , K , Vinorum , K & Whenman , B 2021 , ' Large-Scale Dune Aurora Event Investigation Combining Citizen Scientists' Photographs and Spacecraft Observations ' , AGU Advances , vol. 2 , no. 2 , ARTN e2020AV000338 . https://doi.org/10.1029/2020AV000338

http://hdl.handle.net/10138/332747
https://doi.org/10.1029/2020AV000338

AGU Advances

RESEARCH ARTICLE
10.1029/2020AV000338

Key Points:

- During a dune aurora event spanning over 1,500 km, satellite observations indicate that auroral precipitation takes place in the dune area
- The presence of a mesospheric temperature inversion layer near the dunes provides suitable conditions for mesospheric bore propagation
- The dune propagation speed is estimated for the first time and suggests that strong horizontal winds were present during the event

Supporting Information:

Supporting Information may be found in the online version of this article.

Correspondence to:

M. Grandin,
maxime.grandin@helsinki.fi

Citation:

Grandin, M., Palmroth, M., Whipps, G., Kalliokoski, M., Ferrier, M., Paxton, L. J., et al. (2021). Large-scale dune aurora event investigation combining Citizen Scientists' photographs and spacecraft observations. *AGU Advances*, *2*, e2020AV000338. https://doi.org/10.1029/2020AV000338

Received 30 NOV 2020
Accepted 26 MAR 2021

Author Contributions:

Conceptualization: Maxime Grandin
Data curation: Graeme Whipps, Mark Ferrier, Larry J. Paxton, Martin G. Mlynczak, Jukka Hilska, Knut Holmseth, Kjetil Vinorum, Barry Whenman
Formal analysis: Maxime Grandin
Funding acquisition: Minna Palmroth
Investigation: Maxime Grandin, Milla Kalliokoski, Larry J. Paxton, Martin G. Mlynczak
Methodology: Maxime Grandin
Resources: Minna Palmroth

Large-Scale Dune Aurora Event Investigation Combining Citizen Scientists' Photographs and Spacecraft Observations

Maxime Grandin[1], Minna Palmroth[1,2], Graeme Whipps[3], Milla Kalliokoski[1], Mark Ferrier[3], Larry J. Paxton[4], Martin G. Mlynczak[5], Jukka Hilska[6], Knut Holmseth[7], Kjetil Vinorum[7], and Barry Whenman[3]

[1]Department of Physics, University of Helsinki, Helsinki, Finland, [2]Space and Earth Observation Centre, Finnish Meteorological Institute, Helsinki, Finland, [3]Citizen Scientist, Scotland, UK, [4]The Johns Hopkins University Applied Physics Laboratory, Laurel, MD, USA, [5]Atmospheric Sciences Division, NASA Langley Research Center, Hampton, VA, USA, [6]Citizen Scientist, Finland, [7]Citizen Scientist, Norway

Abstract Recently, citizen scientist photographs led to the discovery of a new auroral form called "the dune aurora" which exhibits parallel stripes of brighter emission in the green diffuse aurora at about 100 km altitude. This discovery raised several questions, such as (i) whether the dunes are associated with particle precipitation, (ii) whether their structure arises from spatial inhomogeneities in the precipitating fluxes or in the underlying neutral atmosphere, and (iii) whether they are the auroral manifestation of an atmospheric wave called a mesospheric bore. This study investigates a large-scale dune aurora event on 20 January 2016 above Northern Europe. The dunes were observed from Finland to Scotland, spanning over 1,500 km for at least 4 h. Spacecraft observations indicate that the dunes are associated with particle precipitation and reveal the presence of a temperature inversion layer below the mesopause during the event, creating suitable conditions for mesospheric bore formation. The analysis of a time lapse of pictures by a citizen scientist from Scotland leads to the estimate that, during this event, the dunes propagate toward the west-southwest direction at about 200 m s^{-1}, presumably indicating strong horizontal winds near the mesopause. These results show that citizen science and dune aurora studies can fill observational gaps and be powerful tools to investigate the least-known region of near-Earth space at altitudes near 100 km.

Plain Language Summary Citizen science recently led to the discovery of a new form of aurora called "the dunes," which consists of a modulation of the brightness in the green diffuse aurora, forming regularly spaced, parallel stripes of brighter emission. This study investigates the nature of the dune aurora by combining photographs taken by citizen scientists and satellite observations during a large-scale event which took place above Northern Europe on 20 January 2016. The dunes were observed from Finland to Scotland, spanning over 1,500 km for at least 4 h. Observations from satellites indicate that the dunes are associated with the precipitation of particles from near-Earth space into the upper atmosphere, and that the atmospheric temperature profile within 60–110 km altitude exhibits features which allow the formation of an atmospheric wave type called "mesospheric bore," which has been suggested as a possible explanation for the dunes' morphology. Finally, the dune propagation speed is estimated for the first time using a timelapse of pictures by a Scottish citizen scientist and suggests the presence of strong horizontal winds in the upper atmosphere.

1. Introduction

Recently, a study carried out jointly by researchers and citizen scientists described an auroral form previously unreported in the literature, which was called "the dunes" (Palmroth, Grandin, Helin, et al., 2020). Citizen science has emerged as a powerful way to unravel previously overlooked physical phenomena while making science accessible beyond academia by involving citizen scientists in research projects (Grandin, 2020). In space physics, a particularly noteworthy illustration of the breakthroughs citizen science can achieve is the ongoing studies of the Strong Thermal Emission Velocity Enhancement (STEVE) phenomenon, which consists of faint optical emissions forming a ribbon equatorward from the main auroral arc, essentially

Visualization: Maxime Grandin
Writing – original draft: Maxime Grandin
Writing – review & editing: Minna Palmroth, Graeme Whipps, Milla Kalliokoski, Mark Ferrier, Martin G. Mlynczak, Kjetil Vinorum

observed at subauroral latitudes, sometimes associated with vertical rays of green emission called "picket fence" (Archer et al., 2019; MacDonald et al., 2018; Semeter et al., 2020).

The dune aurora is also an optical phenomenon, so far mostly reported at subauroral latitudes too, which had not been analyzed in the peer-reviewed scientific literature until it was brought to the attention of the scientific community by citizen scientists. It consists of a modulation of the optical emission intensity within the green diffuse aurora exhibiting an oscillatory pattern in the horizontal dimension. The dunes are rather faint in comparison with auroral arcs. The only scientific study of the dune aurora so far analyzed one particular event and determined that the optical emission associated with the dunes was taking place at about 100 km altitude and that the horizontal wavelength of the dunes was of the order of 45 km (Palmroth, Grandin, Helin, et al., 2020). The study also provided a list including 6 additional reported dune sightings, which were all associated with disturbed geomagnetic conditions corresponding to moderate storms and moderately high substorm activity, and which all took place during the local evening hours within a region characterized by heightened total electron content and located between a pair of upward and downward ionospheric field-aligned currents. During a given event, observational evidence suggests that this phenomenon can persist for tens of minutes to over an hour.

The suggested scenario to explain the morphology of the dune aurora is that it originates from electron precipitation from the magnetosphere in presence of an atmospheric wave in the upper atmosphere. A possible candidate for such a large-scale wave could be a phenomenon known as mesospheric bore (Dewan & Picard, 1998; Smith et al., 2003), which can propagate horizontally in the upper mesosphere in specific conditions. Such conditions are the presence of either a temperature inversion layer (thermal duct) or a wind shear (Doppler duct), which can guide the bore horizontally over large distances (Dewan & Picard, 2001). Although there are indications that the formation of mesospheric bores might involve gravity waves (Dewan & Picard, 2001; Laughman et al., 2009; Seyler, 2005; Yue et al., 2010), the question of the exact mechanism at play is still unresolved (Hozumi et al., 2019).

The proposed theory for the dune aurora formation is that precipitating particles in the suitable energy range (10–20 keV) excite the atomic oxygen at about 100 km altitude in the presence of a mesospheric bore which modulates horizontally the oxygen density. The de-excitation of the oxygen atoms through the emission of photons would then result in diffuse aurora whose brightness is modulated spatially by the inhomogeneous oxygen density. The fact that the dunes have so far always been reported during the local evening hours and in most cases around equinoxes is compatible with the bore scenario, as mesospheric bores show similar occurrence trends (Hozumi et al., 2019; Su et al., 2018).

If proven true, this hypothesis implies that the dune aurora reveals the presence of a mesospheric bore, which is otherwise particularly difficult to observe at auroral latitudes. Indeed, the prime observable to study mesospheric bores is airglow emission, measured either by satellites (Miller et al., 2015; Su et al., 2018), including the National Oceanic and Atmospheric Administration (NOAA) Suomi National Polar-orbiting Partnership (NPP) and Joint Polar Satellite System (JPSS) Day/Night Band sensor (Miller et al., 2013; Seaman & Miller, 2013) or the International Space Station (Hozumi et al., 2018), or by ground-based imagers (Bageston et al., 2011; Fechine et al., 2009). The altitude range within which mesospheric bores and the dunes take place is in fact one of the most challenging regions of near-Earth space when it comes to observations, both through in situ measurements and remote sensing (Sarris, 2019). At the same time, it is a critical interface between the purely neutral and the partly ionized media, between the well-mixed gas and that where species behave independently from one another, as well as a region with complex energetics, dynamics and chemistry due to couplings from above (magnetosphere) and below (lower atmosphere) (Heelis & Maute, 2020; Palmroth, Grandin, Sarris, et al., 2021).

To test the hypothesis that dune aurorae reveal the presence of mesospheric bores, several aspects must be investigated. First, the intrinsically auroral nature of the dunes, that is, that they are the result of excitation of atmospheric constituents by particle precipitation, needs to be confirmed. This requires either direct observations of particle precipitation as performed by low-Earth-orbiting spacecraft or a spectroscopic characterization of the optical emission associated to the dunes. Second, the spatial variations in the precipitating particle fluxes and energies need to be investigated to determine whether the emission modulation associated with the dunes is the result of inhomogeneities in the precipitation or in the underlying atmosphere.

Table 1
Observations of the Dune Aurora Event on 20 January 2016

Location	Photographer	Geographic coordinates	Time (UT)
Aura, Finland	Jukka Hilska	60.621°N, 22.518°E	17:03–17:36
Engerdal, Norway	Knut Holmseth	61.669°N, 12.056°E	20:13
Karmøy, Norway	Kjetil Vinorum	59.382°N, 5.232°E	~20:30
Rattray, Scotland	Graeme Whipps	57.609°N, 1.863°W	19:56–21:51
Lendalfoot, Scotland	Mark Ferrier	55.158°N, 4.959°W	20:27–21:28
Isle of Mull, Scotland	Barry Whenman	56.495°N, 5.971°W	20:57

The last column gives the time interval during which photographs taken by the citizen scientists exhibit dune features.

Third, the coincident observation of dune aurora and a mesospheric bore, or at least evidence that suitable conditions for bore propagation are met in the mesosphere during a dune event, could give strong arguments in favor of the proposed theory.

This paper reports for the first time satellite observations of auroral electron precipitation during a dune event, as well as satellite measurements of middle-atmospheric temperature profiles revealing the presence of temperature inversion layers that could fulfill the necessary conditions for bore propagation. The horizontal phase speed of the dunes is also estimated based on the sole analysis of citizen scientist photographs, and it suggests an unusually large propagation speed which might reveal strong neutral winds at the dune altitude. The studied event took place on 20 January 2016 above Northern Europe; this event is part of the list given in the dune aurora seminal paper (Palmroth, Grandin, Helin, et al., 2020).

2. Data

2.1. Citizen Scientists' Photographs

The pictures of the 20 January 2016 dune aurora event used in this study were collected by six citizen scientists from Finland, Norway and Scotland, between 17 and 22 UT. Table 1 summarizes the dune observations from the six locations during that evening, indicating in each case the name of the photographer, the geographic coordinates of the shooting location, and the time interval during which pictures containing dune aurora features were taken. The given times are expressed in universal time (UT) and are based on the clock of the corresponding camera, recorded in the EXIF files, with two exceptions.

First, the picture taken from Karmøy is part of a video footage whose original individual files could not be retrieved. In such a situation, the only way to estimate the time at which the picture was taken was to make use of the background star field and visually compare it with that given by the Stellarium software (Chéreau, 2020) for the geographic location of the observation. Using this method, the time associated with the picture was estimated to be around 20:30 UT (21:30 Norwegian time), with a likely error of the order of 10 min.

Second, the Rattray footage has been synchronized with that from Lendalfoot, whose clock is, from the photographers' experience, more reliable. The synchronization was done through the visual identification of unambiguous short-lived auroral features which appeared in both footages. The retained time stamps for both footages are those from Lendalfoot, as the corresponding camera is time calibrated more regularly and was found to be less prone to clock drift than the camera in Rattray. A time lapse consisting of 692 images taken at a cadence of 11 s (10 s exposure time + 1 s interval) between 19:55:12 UT and 22:03:05 UT from Rattray is used in this study and is provided in the Supporting Information as Movie S1.

As a last note on the time calibration of the observations, the time stamps of the footage from Aura have been checked to be within about 1 minute accuracy thanks to a satellite trail visible above Ursa Major in a few of the pictures with time stamps between 17:26:29 and 17:26:58 UT (not included in this paper). This trail matches with a SL-16 R/B satellite overpassing in the same direction in the same region of the sky one

minute earlier as given by the In-The-Sky.org website (https://in-the-sky.org/) using orbital elements from 20 January 2016.

2.2. Satellite Observations

2.2.1. Solar Wind Observations and Geomagnetic Indices

Solar wind data and geomagnetic indices during the 20 January 2016 event were retrieved at 5 min resolution from the OMNIWeb database (King & Papitashvili, 2005) to provide context for the event. The solar wind data provided through OMNIWeb are in situ observations by the Advanced Composition Explorer (ACE) and Wind spacecraft at the Lagrangian L1 point of the Sun–Earth system, which have been propagated in time to the terrestrial bow shock.

Two geomagnetic indices, available from OMNIWeb, are considered to quantify geomagnetic activity during the event. The Auroral Electrojet (AE) index (Davis & Sugiura, 1966) is calculated from ground-based magnetometer observations at auroral-latitude stations in the northern hemisphere. It is a proxy for substorm activity. The SYM-H index (Iyemori, 1990) is calculated from magnetometer measurements at midlatitude stations; it is used as a proxy for geomagnetic storm activity. AE and SYM-H are maintained by the World Data Center for Geomagnetism at Kyoto Observatory.

2.2.2. Electron Precipitation Observations

The Special Sensor Ultraviolet Spectrographic Imager (SSUSI), on board spacecraft from the Defense Meteorological Satellite Program (DMSP) series on Sun-synchronous orbit at about 830 km altitude, is a remote-sensing instrument measuring optical emissions from the upper atmosphere and ionosphere in the far-ultraviolet wavelength range (80–170 nm) (Paxton et al., 2002). As the satellite is moving along its orbit, a scanning imaging spectrograph performs limb-to-limb scans, resulting in the measurement of the far-ultraviolet spectrum in a ∼3,000 km-wide band across the spacecraft track (Paxton et al., 2017). In the auroral regions, these observations are mapped to an altitude of 110 km, enabling the estimation of auroral electron precipitation integral energy flux and mean energy in the polar regions. Since the auroral emissions observed by SSUSI take place within a relatively thin altitude range (e.g., Lee et al., 2010), parallax effects in mapping the observations to 110 km can be neglected, except at the very edge of the swath. A detailed description of the SSUSI instrument and its data products can be found in Paxton et al. (1993).

In this study, we use the integral energy flux and mean energy of precipitating electrons inferred from SSUSI observations by the DMSP-F19 spacecraft during the dune aurora event, as the satellite made an overpass above Fennoscandia around 17:20 UT, providing a suitable cross-track scan of the auroral region above Northern Europe.

2.2.3. Mesospheric Temperature Observations

The Sounding of the Atmosphere using Broadband Emission Radiometry (SABER) instrument onboard the Thermosphere Ionosphere Mesosphere Energetics Dynamics (TIMED) spacecraft consists of an infrared radiometer performing limb scans of the middle atmosphere to measure emissions in the 1.27–17 μm wavelength range (Russell et al., 1999). Among the data products which can be derived from such measurements, altitude profiles of the neutral temperature are obtained in the mesosphere. In this study, we use temperature profiles in the middle atmosphere above Northern Europe measured by SABER on 20 January 2016 between 21:43:12 UT and 21:47:16 UT.

3. Results

3.1. Dune Observations by Citizen Scientists

Figure 1 presents six examples of photographs by citizen scientists from Finland (Figure 1a, Aura), Norway (Figure 1b, Engerdal; Figure 1c, Karmøy), and Scotland (Figure 1d, Isle of Mull; Figure 1e, Lendalfoot; Figure 1f, Rattray). The shown pictures were taken between 17:23 UT (19:23 Finnish local time) and 21:15 UT (21:15 Scottish local time). All photographs feature relatively diffuse green emission exhibiting patterns evoking a wavefield, in a similar way as in the first report of dune aurora (Palmroth, Grandin, Helin,

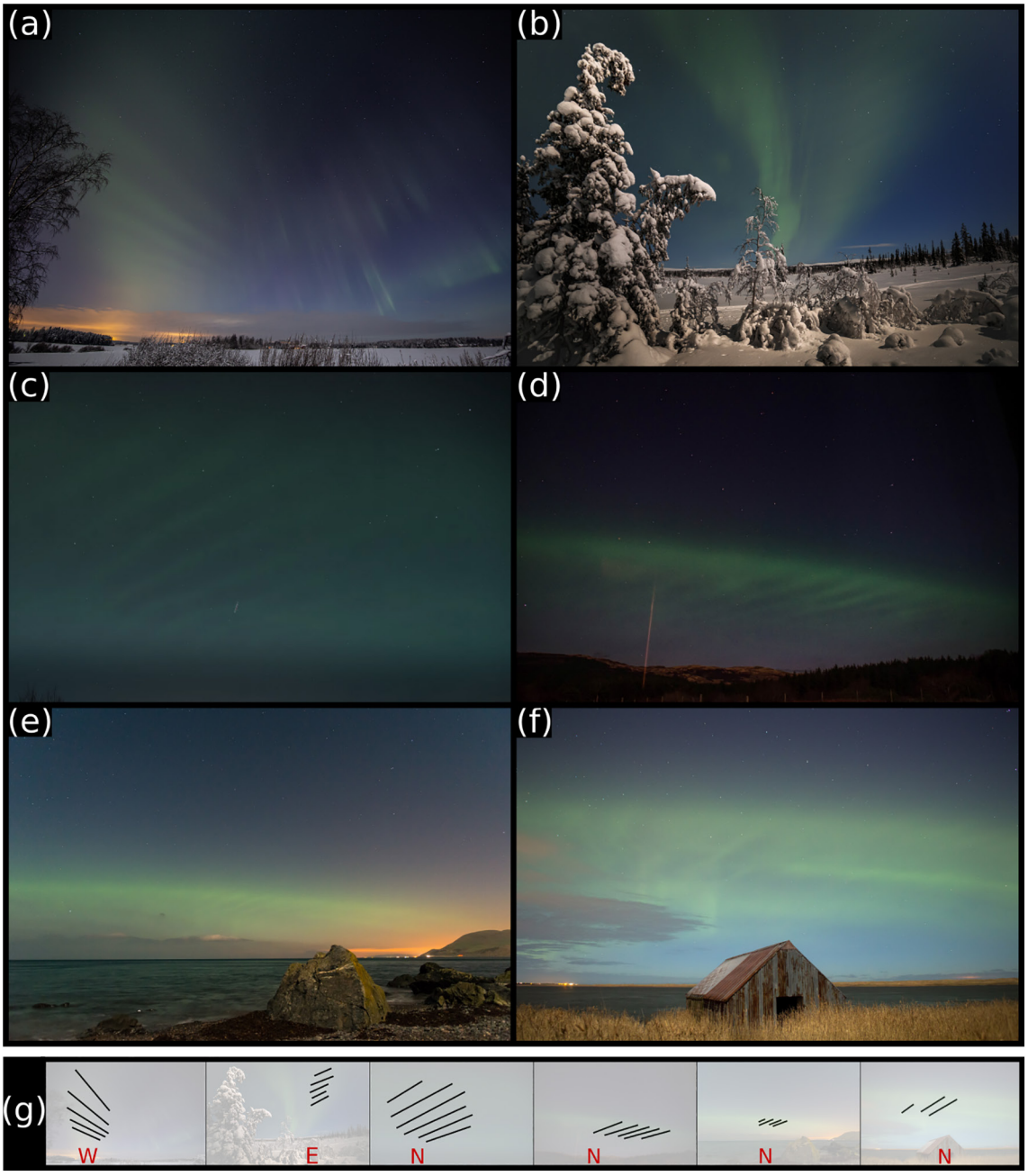

Figure 1. Selected pictures of the dune aurora by Citizen Scientists during the 20 January 2016 event. The pictures were taken from (a) Aura, Finland, at 17:23 UT, (b) Engerdal, Norway, at 20:13 UT, (c) Karmøy, Norway, around 20:30 UT, (d) the Isle of Mull, Scotland, at 20:57 UT, (e) Lendalfoot, Scotland, at 21:15 UT, and (f) Rattray, Scotland, at 21:15 UT. (g) The same pictures, in the same order, with indications of the cardinal directions (N: north, W: west, E: east) and of the dune elements which are mapped in Figure 2.

et al., 2020). In some of the pictures (Figures 1a and 1f), discrete auroral forms such as arcs or pillars can be seen poleward of the dunes. The nearly vertical line in Figure 1d is likely a reflection internal to the camera, and is not a geophysical feature.

The six locations from which the dunes were photographed on 20 January 2016 are indicated on the map given in Figure 2. The locations of the dunes identified in the pictures shown in Figure 1 were determined by looking at their positions relative to background stars whose azimuth and elevation angles were obtained using the Stellarium software (Chéreau, 2020), assuming that the optical emissions associated with

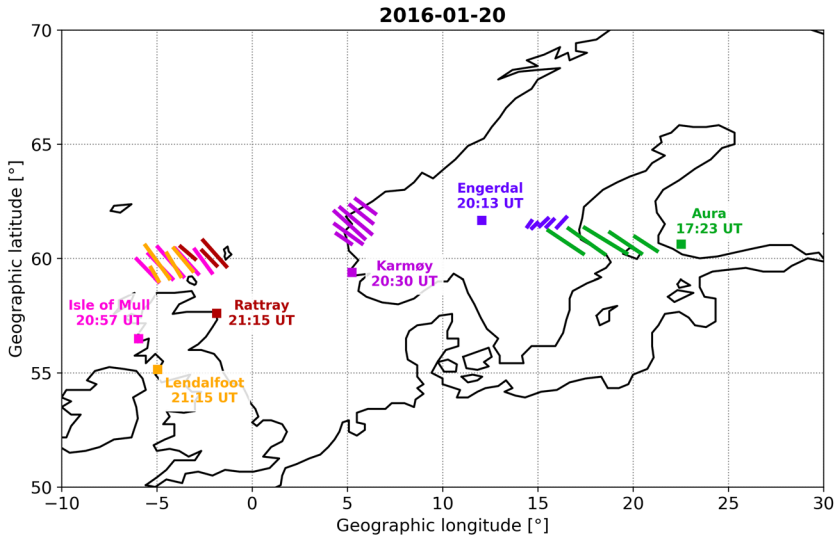

Figure 2. Mapping of the dunes on 20 January 2016 across Northern Europe. For each location, one picture was selected for the mapping; the corresponding time is indicated in UT. The altitude of the dunes is assumed to be 100 km.

the dunes were taking place at 100 km altitude. The detailed methodology and the related equations can be found in the dune aurora discovery paper (Palmroth, Grandin, Helin, et al., 2020). The obtained dune locations are indicated in Figure 2.

Apart from the dunes photographed from Engerdal (Figure 1b), the wave fronts have an orientation along the northwest–southeast direction. Possible explanations for the different orientation of the dunes seen from Engerdal will be presented in the Discussion section. Overall, the dune aurora sightings during that night cover an area extending for nearly 1,500 km in the east–west direction, but only about 400 km in the north–south direction. The horizontal wavelength of the dunes observed during the event is estimated using a slightly improved method compared to that described in Palmroth, Grandin, Helin, et al. (2020) (see Appendix A) and is found to be about 42 ± 1.4 km (Aura), 30 ± 1.5 km (Karmøy), 38 ± 14 km (Lendalfoot), and 41 ± 5.3 km (Isle of Mull), comparable to that of the dune event reported in the Palmroth, Grandin, Helin, et al. (2020) study.

3.2. Geomagnetic Conditions During the Event

Context for the studied dune aurora event is given in Figure 3, which shows the solar wind driving conditions as well as two geomagnetic indices on 20 January 2016. Figure 3a displays the interplanetary magnetic field (black line) and its north–south component (B_z, red line), which reveal that the interplanetary magnetic field magnitude was fairly large (about 15 nT throughout the day) and was mostly oriented southward between 5 and 21 UT ($B_z \approx -10$ nT). Such conditions are known to produce magnetic reconnection at the dayside magnetopause and subsequently drive nightside reconnection in the magnetotail, which leads to spectacular auroral displays at high latitudes (Dungey, 1961). While the solar wind speed (Figure 3b) was slightly below its average value of 400 km s^{-1} (Richardson & Cane, 2012), the number density (Figure 3c) was of the order of 20 proton cm^{-3} (median value: 6.6 proton cm^{-3}; Hundhausen et al., 1970) and the solar wind proton temperature (Figure 3d) was close to 100 kK (which is roughly equal to its median value of 8.9 eV at 1 AU, according to Wilson et al., 2018) at the time when the dunes were observed (~17:00–21:30 UT). This solar wind flow corresponds to an interplanetary coronal mass ejection and is identified as such in the catalog by Richardson and Cane (Cane & Richardson, 2003; Richardson & Cane, 2010).

This interplanetary coronal mass ejection produced a geomagnetic storm, as is illustrated by the SYM–H index (Figure 3e, red line) reaching negative values down to almost −100 nT around 17 UT (quiet-time values are near zero). The dunes therefore took place toward the end of the main phase of the storm, as the recovery phase, indicated with increasing SYM-H values, started around 22 UT. Finally, the auroral electrojet (AE) index (Figure 3e, black line) exhibits elevated values of the order of 800 nT during the dune aurora

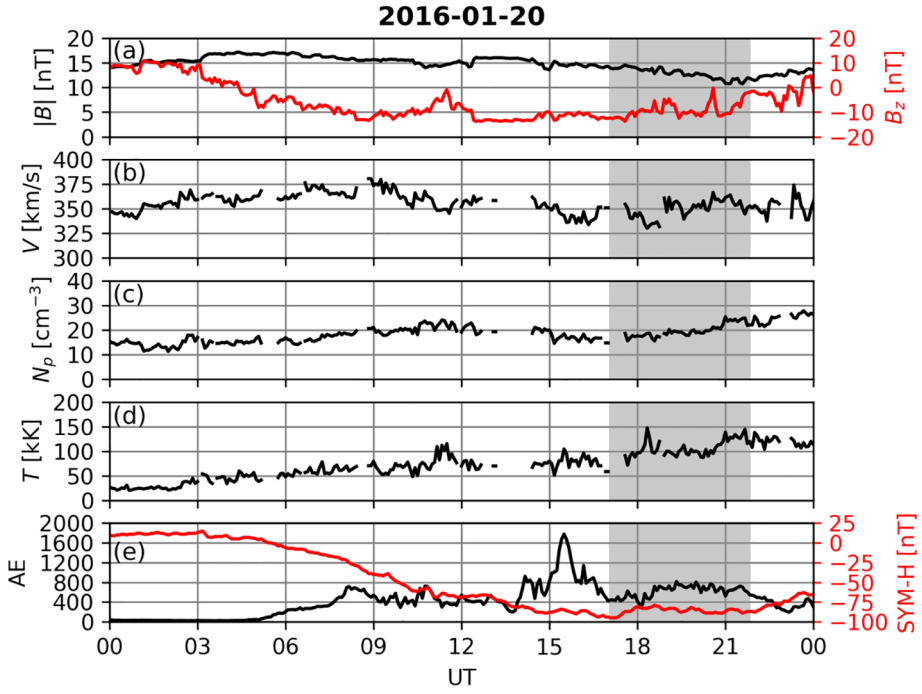

Figure 3. Solar wind parameters and geomagnetic conditions on 20 January 2016. (a) Interplanetary magnetic field magnitude (black) and north-south component (red). (b) Solar wind speed. (c) Solar wind density. (d) Solar wind temperature. (e) Auroral electrojet (AE, black) and SYM-H (red) indices. The time interval during which dunes were observed by citizen scientists is indicated with gray shading.

observations (quiet-time values are near zero), revealing sustained substorm activity consistent with the observation of auroral displays at high latitudes in the evening sector.

3.3. Satellite Observations of Particle Precipitation

One of the first questions which arose from the first dune aurora study (Palmroth, Grandin, Helin, et al., 2020) was whether the dunes are intrinsically an auroral phenomenon, that is, associated with the precipitation of particles from the magnetosphere, or if they might be the result of the excitation of atmospheric constituents by local processes in the ionosphere, as is suspected for the optical phenomenon called STEVE (Strong Thermal Emission Velocity Enhancement) which can be observed at subauroral latitudes (Gallardo-Lacourt et al., 2018; Harding et al., 2020; Mende et al., 2019; Semeter et al., 2020).

Figure 4 presents observations of electron precipitation above Northern Europe on 20 January 2016 around 17:20 UT by the SSUSI instrument on board the DMSP-F19 satellite. Figure 4a shows the inferred energy flux of precipitating electrons, while Figure 4b gives their mean energy. In both panels, the location of the dunes observed from Aura at 17:23 UT (Figure 1a, which was closest in time to the satellite overpass among the footage) as shown in Figure 2 is indicated with white lines. A white star marks the position of DMSP-F19 at 17:20 UT, which is the time near which the SSUSI cross-track scan of the dune aurora region took place. In the bottom-left-hand corner of each panel, a zoomed-in box enables a closer inspection of the electron precipitation characteristics in the area where the dunes were observed.

The SSUSI observations suggest that the dunes occur at the equatorward edge of the auroral precipitation area. This region is characterized by a relatively low energy flux, of the order of 1–8 mW m^{-2}, compared to auroral arcs which can be identified at higher latitudes, with energy fluxes of 30 mW m^{-2} or greater. On the other hand, the mean energy of the precipitating electrons within the equatorward edge of the auroral region appears overall higher than the ~5–8 keV values seen poleward from it. The area to which the dunes are mapped is located partly on top and partly south of a cluster of pixels indicating ~20 keV electron mean energy (the maximum value derived from SSUSI observations). The dunes themselves are partly mapped

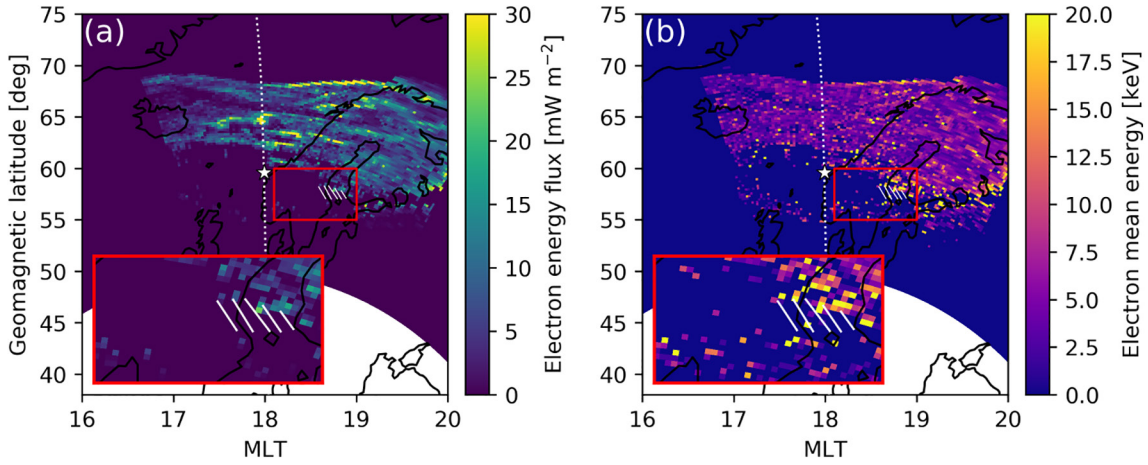

Figure 4. Observed auroral precipitation by the SSUSI instrument onboard DMSP-F19 during the dune event. (a) Integral energy flux of electron precipitation. (b) Mean precipitating energy. The DMSP-F19 track is shown with a thin dotted line, while a white star indicates the position of the spacecraft at 17:20 UT. The white stripes indicate the location of the dunes photographed from Aura at 17:23 UT (see Figure 2). The red rectangle shows the area of which a zoomed-in box is reproduced in the bottom-left-hand corner of each panel. DMSP, Defense Meteorological Satellite Program; SSUSI, Special Sensor Ultraviolet Spectrographic Imager.

to a region where the electron precipitation characteristics were not derived because of coincident strong proton precipitation fluxes. This suggests that the region where dunes are observed from Aura is associated with the precipitation of auroral electrons, of which a significant number are likely to have their energies within the 10–20 keV range, but a possible role of precipitating protons cannot be excluded. Incident electrons with energies within this range are expected to deposit most of their energy within 98–106 km altitude (Berger et al., 1970). This is consistent with the altitude of the dunes determined by triangulation from two simultaneous pictures in another event (Palmroth, Grandin, Helin, et al., 2020), and supports the assumption used for their mapping from photographs (Figure 2). While direct observations of precipitating electron fluxes with in situ particle detectors are not available above the dunes, the Special Sensor J (SSJ) instrument onboard DMSP-F19 did measure local precipitating particle fluxes along the satellite's orbit (dotted line in Figure 4). The instrument measured an enhancement in the differential fluxes of precipitating electrons at energies comprised between 1 and 10 keV when the satellite was flying at ~57.5–58.0 MLAT, that is, at the same geomagnetic latitudes as the dunes, but about 600 km west from them, as well as large precipitating proton energy fluxes, consistent with the absence of SSUSI derived electron products in that area (not shown). Since the spacecraft was flying at earlier MLTs and since the dune observations are within the dusk sector of the auroral oval, which likely exhibits sharp longitudinal gradients, it is not possible to conclude whether a similar particle detector flying right above the dunes would have observed an enhancement in electron fluxes affecting energies not limited to 1–10 keV but also including a >10 keV contribution.

3.4. Mesospheric Temperature Inversion Layer

Our working hypothesis to explain the morphology of the dune aurora is that it could be associated with a large-scale atmospheric wave called a mesospheric bore modulating the density of the oxygen near the mesopause (Palmroth, Grandin, Helin, et al., 2020). Mesospheric bores are known to propagate within a narrow waveguide caused by either a temperature inversion layer or a wind shear below the mesopause (Fechine et al., 2009; She et al., 2004).

Figure 5 presents mesospheric temperature altitude profiles measured by the SABER instrument on board the TIMED satellite during the dune aurora event. The atmospheric soundings took place between 21:43:12 and 21:47:16 UT, during which five successive profiles were inferred from observations whose tangent point locations are indicated in Figure 5a. The profiles were obtained close to the region where the dunes were seen from Karmøy (shown in green in this figure), about 1.25 h earlier. The retrieved temperatures are given in Figures 5b–5f, with a color code matching that of the locations indicated on the map. The profiles are shown between 60 and 110 km altitude, with total root-sum-squared (one-sigma) uncertainties (horizontal

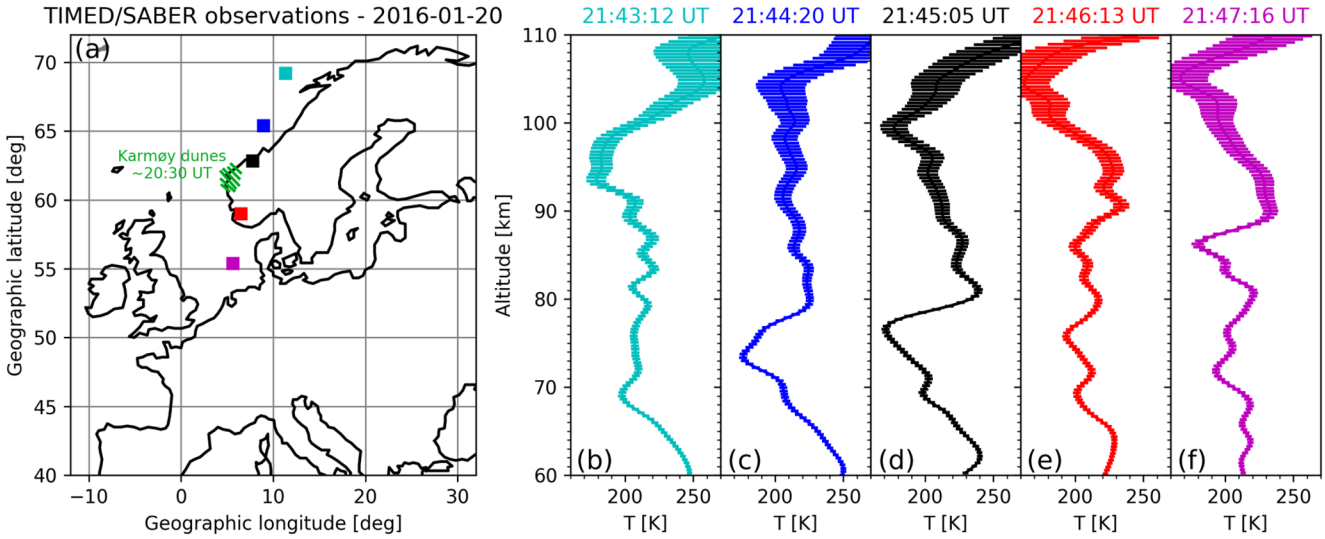

Figure 5. Observed atmospheric temperature profiles by the SABER instrument onboard TIMED during the dune event. (a) Locations of the temperature profile measurements between 21:43:12 and 21:47:16 UT. (b)–(f) Corresponding temperatures profiles, color-coded to match the squares in panel (a). Horizontal bars along the profiles indicate the one-sigma uncertainties associated with the retrieved temperatures. The location of the dunes seen from Karmøy around 20:30 UT is shown in green. SABER, Sounding of the Atmosphere using Broadband Emission Radiometry; TIMED, Thermosphere Ionosphere Mesosphere Energetics Dynamics.

bars, combining random and systematic errors; see García-Comas et al., 2008, for more details) as obtained by linear interpolation of the tabulated values given in the SABER documentation (http://saber.gats-inc.com/temp_errors.php, Table 1).

Identifying the mesopause by finding the minimum temperature above 80 km altitude, one can see that the mesopause lies at about 93 km altitude at the highest-latitude location (Figure 5b) whereas it is located between 99 and 105 km altitude in the other four profiles. Additionally, at those four locations, complex mesospheric temperature profiles with distinct temperature inversion layers can be identified: within 73–79 km altitude (Figure 5c), within 77–81 km altitude (Figure 5d), within 86–91 km altitude (Figure 5e), and within 86–90 km altitude (Figure 5f). Additional less prominent temperature inversion layers can be seen in those profiles, but we do not focus on these in this study. The temperature increases in the above-mentioned inversion layers are of the order of 35–70 K, which are values significantly larger than the uncertainties on SABER temperature measurements and of the same order or greater than reported in past studies of mesospheric inversion layers (e.g., Hauchecorne et al., 1987; Smith et al., 2017; Yuan et al., 2014). Inversion layers in the mesosphere can last for up to several days and extend across over 500 km (Hauchecorne et al., 1987); therefore, one can reasonably expect that the SABER observations can provide insight into the mesospheric conditions associated with the dune event.

While the presence of a temperature inversion layer below the mesopause does not necessarily imply that a mesospheric bore was indeed propagating in the upper mesosphere, these observations reveal the presence of a waveguide within which a bore can propagate. This supports the scenario that dune aurora might be the optical manifestation of electron precipitation into a horizontally structured upper atmosphere whose properties are affected by a mesospheric bore. Moreover, the increasing altitude of the temperature inversion layer as the atmospheric soundings were performed more and more southward suggests that the ducting layer altitude would likely increase with decreasing latitude. This will be further analyzed in the Discussion section.

3.5. Dune Propagation Speed

Earlier reports of dune aurora indicated that the wavefield can appear to have a drift with a component perpendicular to the wavefront orientation (Palmroth, Grandin, Helin, et al., 2020). The time lapse of auroral pictures taken from Rattray with a fixed camera orientation from 19:55 to 22:03 UT (given in Supporting

Information as Movie S1), wherein the dunes can be identified between 19:56 and 21:51 UT, indicates that the dunes were drifting toward the left (and slightly toward the top) in the images, corresponding to an overall westward (and slightly southward) motion given the pointing direction of the camera. This time lapse can therefore be used to estimate the drift speed of the wavefield during the 20 January 2016 event. Figure 6a shows a photograph from this footage, taken at 21:03:04 UT, in which several dune wave fronts are prominent. Figures 6b and 6c present keograms constructed from the 1000th (central, indicated in red in Figures 6a) and 1500th (indicated in blue) columns of pixels, starting from the left, in the time lapse images. The time interval when the dunes were the clearest in the area of the images close to the selected columns of pixels can be identified in the keograms, as the drifting dunes appear as slightly slanted parallel stripes in Figures 6b and 6c. This interval starts around 20:45 UT and lasts until about 21:15 UT.

During this time interval, time series of the difference between the signal in the green and the blue channels in a selected pointing direction (626th row of pixels, starting from the top, indicated with black lines in the keograms) are extracted from Figures 6b and 6c and displayed in Figures 6e and 6f, respectively. The reason for displaying this parameter is simply that the dunes are prominent in the green channel, whereas the background sky is best rendered by the blue channel; hence, the difference between green and blue enhances the contrast contained in the dunes. Distinct pseudo oscillations in these signals reveal the drifting motion of the dunes during the selected time interval.

Since the selected line of pixels in either keogram corresponds to the time variation of the light received from a fixed pointing direction in the sky, the pseudo-periodicity exhibited in the signal plotted in the corresponding bottom panel of Figure 6 is the result of the transit of successive bright bands of the dunes in the observed portion of the sky. In Figure 6d, nine periods can be counted between 20:45 and 21:11 UT, which yields the value of 2.9 ± 0.1 min for one period. Correspondingly, Figure 6e exhibits eight periods between 20:45 and 21:12 UT, which yields 3.4 ± 0.1 min for one period (see Appendix A for more details on the uncertainty estimation).

The 2D images only provide a projection of the dunes, which are intrinsically a three-dimensional phenomenon. However, under the assumption that the motion of the dunes takes place in the horizontal plane and that the wave fronts are orthogonal to the wave vector, it is possible to obtain a rough estimate of the propagation speed of the dunes by simply dividing their wavelength by the above-estimated periods. The mapping of the dune field photographed from the Isle of Mull at 20:57 UT (shown in magenta in Figure 2), that is, near the middle of the studied time interval, leads to an estimated wavelength of the dune field of 41 ± 5.3 km (see Appendix A). Eventually, the speed of propagation of the dunes with respect to the observer in Rattray is estimated to be of the order of 237 ± 32 m s^{-1} when considering a 2.9 ± 0.1 min period and 202 ± 27 m s^{-1} when considering a 3.4 ± 0.1 min period. This propagation speed is likely the combination of the motion of the dunes with respect to the neutral gas and the neutral wind with respect to an observer on the ground.

4. Discussion

Since the dune aurora was first presented in the literature (Palmroth, Grandin, Helin, et al., 2020), key questions regarding its nature have arisen. The combination of ground-based observations provided by numerous dune photographs by citizen scientists from locations spanning over most of Northern Europe with measurements by calibrated scientific instruments on board low-Earth-orbiting spacecraft has brought a few elements addressing those questions.

First, the SSUSI data shown in Figure 4 suggest that the dunes are indeed an auroral phenomenon, being associated with electron precipitation. The mean precipitating electron energy in the area where dunes were observed from Aura is expected to have strongest effects in the 98–106 km altitude (Berger et al., 1970), which is consistent with the altitude inferred by a triangulation method in a different dune event (Palmroth, Grandin, Helin, et al., 2020). Yet, the equatorward part of the region to which the dunes were mapped exhibits some gaps in the SSUSI data. This is due to coincident high precipitating proton fluxes which prevent retrieving the local electron precipitation energies. Nevertheless, one cannot entirely rule out that other processes leading to optical emission in the dunes might take place. Additional observational evidence could enable one to be entirely conclusive regarding the association of dunes with particle precipitation

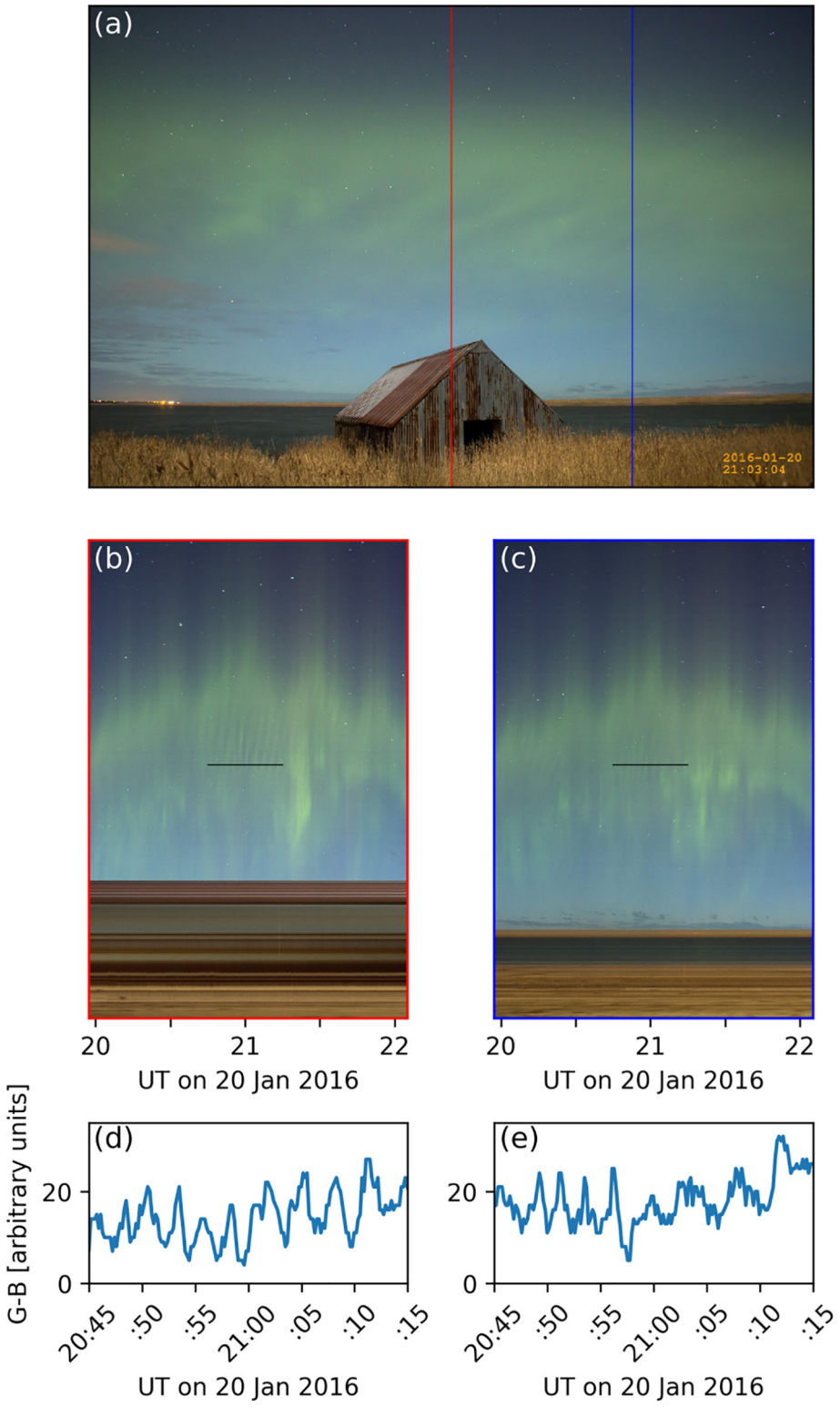

Figure 6. Analysis of images of the aurora from a time lapse taken from Rattray, Scotland. (a) Image taken at 21:03:04 UT with 10 s exposure. The red and blue lines indicate the columns of pixels used to generate the keograms shown in panels (b) and (c), respectively. (d) Time series of the difference between the green and blue pixel values at the location indicated with a black line in panel (b). (e) Same for the pixels indicated with a black line in panel (c).

rather than resulting from excitation of oxygen atoms by other sources such as suprathermal electrons (Semeter et al., 2020). For instance, spectroscopic analysis of the emission from the dune field could determine whether the emission spectrum is consistent with excitation by precipitating particles, as was done to investigate the mechanism behind the STEVE optical emissions (Gillies et al., 2019; Mende et al., 2019). This would require dune observations by suitably calibrated spectrometers, which are not available during this event.

Besides, the available data during this event do not allow to determine whether the large-scale structure of the dunes as a wavefield with spatially modulated optical emission intensity is due to a spatial modulation of the precipitating electron flux properties (number flux, energy flux, and energy spectrum), by processes which could take place either in the magnetosphere or above the ionosphere, or to spatial inhomogeneities in the upper atmosphere in presence of a wave such as a mesospheric bore. To find conclusive evidence regarding the presence of a mesospheric bore in the region where the dunes were observed, one would need data from a day-night band (DNB) instrument such as is part of the Visible Infrared Imaging Radiometer Suite (VIIRS) on board the Suomi National Polar-orbiting Partnership (Suomi-NPP) satellite (Li et al., 2019; Miller et al., 2012, 2013, 2015; Su et al., 2018) or from ground-based airglow imagers (Bageston et al., 2011; Fechine et al., 2009; Li et al., 2019).

Nevertheless, the SABER data shown in Figure 5 indicate that temperature inversion layers were present in the mesosphere above southern Norway around 21:45 UT, that is, at a time when dune aurora was still observed from Scotland, about 300 km west from the tangent point of temperature profile measurements, and only 1.25 h after dunes were observed from Karmøy close to the sounding points. Highly similar mesospheric temperature profiles have been observed, also by SABER, in the presence of a mesospheric bore (Li et al., 2019), which suggests that mesospheric conditions during the 20 January 2016 dune aurora event might have been suitable for bore propagation, as a thermal duct which could have acted as a waveguide was present in the mesosphere. The fact that this duct exhibits increasing altitude with decreasing latitude could constrain the dunes to be visible only at latitudes where a putative mesospheric bore affects the oxygen density in the suitable altitude range. This is consistent with the absence of dune aurora reports beyond ~63°N geographic latitude, as the thermal duct was there too low for the auroral (~100 km) altitude region to be modulated by a bore.

Additional evidence compatible with the hypothesis that a bore did propagate in the ducting layer formed by the temperature inversion layer is the presence of unstable regions near the dune altitude. Figure 7 presents potential temperature and squared Brunt–Väisälä frequency profiles calculated from the temperatures retrieved during the five SABER soundings shown in Figure 5. The potential temperature is given by

$$T_{\mathrm{pot}} = T\left(\frac{P_{\mathrm{std}}}{P}\right)^{\frac{2}{7}}, \tag{1}$$

with T and P the temperature and pressure obtained from the SABER soundings, and P_{std} the standard pressure (here, we used the usual value of 1,000 mbar). The squared Brunt–Väisälä frequency is calculated as

$$N^2_{\mathrm{BV}} = \frac{g}{T}\left(\frac{\mathrm{d}T}{\mathrm{d}z} + \Gamma_d\right), \tag{2}$$

where g is the acceleration due to gravity, Γ_d the dry adiabatic lapse rate, and z the altitude. We use values of $g = 9.55\ \mathrm{m\ s^{-2}}$ and $\Gamma_d = 9.5\ \mathrm{K\ km^{-1}}$ in the upper mesosphere. Looking at altitudes close to 100 km, where the dunes are assumed to occur, one can see that convectively unstable regions exist within this altitude range at the locations close to the Karmøy dune sighting (Figures 7c, 7d, 7h, and 7i). This is illustrated by the negative vertical gradients in the potential temperature profiles and the negative values of N^2_{BV}, which reveal superadiabatic conditions close to the mesopause. In an event study, Yuan et al. (2014) noted the presence of a superadiabatic atmospheric region a few kilometers above a mesospheric inversion layer and suggested that it could have been formed following the propagation of a bore in the upper mesosphere. The presence of convectively unstable regions within 98–100 km altitude near the location where the dunes were observed

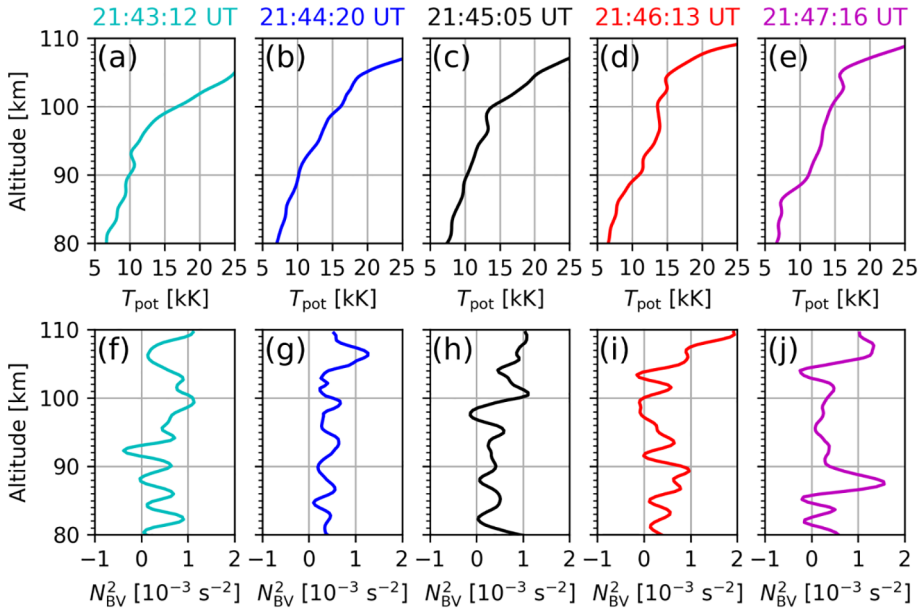

Figure 7. (a)–(e) Potential temperatures profiles calculated from the five SABER soundings considered in Figure 5 using Equation 1, color-coded to match the squares in Figure 5a. (f)–(j) Corresponding squared Brunt–Väisälä frequency profiles calculated using Equation 2. SABER, Sounding of the Atmosphere using Broadband Emission Radiometry.

from Karmøy is therefore compatible with the mesospheric bore scenario, although this is not enough to conclude on the possible presence of a mesospheric bore during the 20 January 2016 dune event.

The estimated properties of the dune field are also consistent with those of mesospheric bores. The observed horizontal wavelengths of the dunes are comprised between 30 ± 1.5 km (dunes observed from Karmøy) and 42 ± 1.4 km (dunes observed from Aura). Those values are very similar to those found in the study of two mesospheric bores above Europe, where the horizontal wavelength of the bores were 34.7 ± 3.7 and 34.4 ± 6.3 km (Smith et al., 2017). In addition, the vast area within which dune aurorae were spotted during this event (~1,500 km in longitude and ~400 km in latitude) is in good agreement with typical mesospheric bore widths (Su et al., 2018) and the horizontal distances they can cover (e.g., Smith et al., 2003).

It has been found in a study of a mesospheric bore above the Tibetan plateau that a given bore can exhibit variability in the horizontal wavelength of its trailing undulations (between 27 ± 5.3 and 45 ± 4.6 km in that case), that variation being attributed to a change in the depth of the duct within which the bore was propagating (Li et al., 2019). Similarly, the bore phase speed exhibited variations and was comprised between 60 ± 8.4 m s^{-1} and 87 ± 10.3 m s^{-1}. Other studies have reported intrinsic mesospheric bore velocities close to or exceeding 100 m s^{-1} (Hozumi et al., 2018; Smith et al., 2017). The phase speed of the dunes derived from the analysis of the Rattray footage, on the other hand, was significantly higher, with an estimated value of the order of 202(±27)–236(±32) m s^{-1}. A possible explanation for this large difference can be the effect of horizontal winds. Indeed, in the case of the mesospheric bore observed above Tibet (Li et al., 2019), mesospheric wind observations showed that the bore was propagating in a direction roughly orthogonal to that of the neutral winds, which therefore had only a minor contribution to the bore phase speed. In contrast, a case of mesospheric bore over Europe propagating antiparallel to the neutral wind led to an observed bore speed significantly lower than its intrinsic speed of ~130 m s^{-1} (Smith et al., 2017).

Neutral wind measurements in the relevant region are not available for the 20 January 2016 dune event, hence it is not possible to determine whether sufficiently strong westward mesospheric winds could account for the large phase speed of the dunes observed with respect to the ground. Typically, the zonal winds near the mesopause are rather weak in January at European high latitudes, with on average 20 m s^{-1} values or less in the eastward direction in Sodankylä (67°N) (Lukianova et al., 2018). However, it has been shown that, during moderate substorms, the zonal component of thermospheric winds can reach large

(~200 m s^{-1}) westward values in response to the increased geomagnetic activity (Cai et al., 2019) and, in particular, strong westward winds can occur in association with subauroral polarization streams (SAPS) in the duskside thermosphere (Ferdousi et al., 2019; Wang et al., 2012). Those latter studies, however, investigated neutral winds at higher altitudes than that of the dunes, where wind velocities are typically larger than in the lower thermosphere/upper mesosphere. Nevertheless, neutral wind speeds greater than 100 m s^{-1} can be observed near the dune altitude at high latitudes (Ishii et al., 1999; Nygrén et al., 2015); hence, the large phase speed values estimated for the dune wavefield could be explained by the combination of the bore speed in the neutral gas frame and large neutral winds in the lower thermosphere/upper mesosphere.

Another aspect which might be explained by the neutral winds is the fact that the dunes photographed from Engerdal have a different orientation compared to all other observations during the 20 January 2016 event (see Figure 2). The Engerdal dunes are spatially located fairly close (~100 km) to those observed from Aura but are separated in time from this earlier sighting by almost 3 h. Less than 20 min later, dune aurora with the same orientation as that seen from Aura was photographed from Karmøy, about 500 km further west. Assuming that the dunes are indeed associated with a mesospheric bore, this means that the latter had likely almost reached the Norwegian coast when the Engerdal dunes were observed. It is therefore plausible that the dunes seen from Engerdal, which are the least well-defined among the photographs (see Figure 1), could reveal a remnant of the mesospheric bore with wave fronts whose location and orientation have been affected by sheared neutral winds. It is, however, difficult to go beyond speculation in the absence of neutral wind measurements near the mesopause altitude.

More importantly, a fundamental question raised by this study is that of the plausibility of bore-induced oxygen density variations having a sufficient amplitude at the altitude where the auroral emissions take place (assumed to be 100 km, i.e., more than 10 km above the temperature inversion layer detected by SABER soundings) for a modulation in the auroral emissions to be detectable in citizen scientist photographs. One option to investigate this would be to carry out numerical simulations of auroral emission intensity resulting from a given flux and characteristic energy of electron precipitation into a neutral atmosphere disturbed by the propagation of a mesospheric bore. Such simulations could test various bore propagation altitudes to determine (i) whether the suggested mechanism can indeed produce the dunes and (ii) if so, how stringent the requirements on the bore altitude and amplitude as well as on the electron precipitation properties are to lead to the appearance of the dunes. Pioneering works undertaking to relate auroral emissions and atmospheric composition (e.g., Hecht et al., 1989, 1991; Strickland et al., 1989) could suggest a suitable approach to tackle this question. Another key hypothesis to investigate, especially in modeling studies, is whether mesospheric bores could themselves be triggered by electrodynamical processes associated with magnetosphere–ionosphere–thermosphere couplings, as was conjectured in Palmroth, Grandin, Helin, et al. (2020).

Finally, one can mention that, while mesospheric waves are inherently difficult to study due to the scarcity of available observations, the emergence of new optical phenomena possibly revealing them might provide new methods to improve the understanding of mesospheric bores, and more generally acoustic-gravity waves, in the middle atmosphere. The dune aurorae are one such example, and in a conference paper, Roldugin et al. (2016) describe possible signatures of acoustic-gravity waves in the aurora. In addition, mesospheric wave signatures have also been noted in other types of optical emissions. While airglow emissions have been the most widely used proxy for such studies (e.g., Bageston et al., 2011; Dewan & Picard, 1998; Hozumi et al., 2018; Li et al., 2019; Miller et al., 2015), one can also note that transient luminous events known as elves (Emissions of Light and Very Low Frequency Perturbations due to Electromagnetic Pulse Sources) have been found to exhibit striated structures revealing the presence of gravity waves (Yue & Lyons, 2015).

5. Conclusions

This study investigated a dune aurora event which took place in the local evening hours of 20 January 2016 above Northern Europe. The dunes were photographed by six citizen scientists from various locations in Finland, Norway, and Scotland, between 17:03 and 21:51 UT. Overall, dune aurorae were visible for over 4 h in a region whose longitudinal and latitudinal extents span across nearly 1,500 and 400 km, respectively.

Observations from the SSUSI imager on board the DMSP-F19 spacecraft revealed that the dunes occurred in a region where electron precipitation took place with relatively low energy fluxes (1–8 mW m^{-2}) and a mean energy larger than at more poleward latitudes, including >10 keV electrons which can produce auroral emissions at about 100 km altitude. A possible role of proton precipitation needs to be investigated in future studies.

In addition, neutral temperature profiles retrieved by SABER on board the TIMED satellite showed that temperature inversion layers were present in the mesosphere in the vicinity of the dunes, thus creating suitable conditions for the formation and propagation of a mesospheric bore, which was suggested as a possible explanation for the morphology of the dunes in the discovery paper (Palmroth, Grandin, Helin, et al., 2020).

Finally, the analysis of a time lapse created from the footage recorded by one of the citizen scientists enabled the estimation of the propagation speed of the dunes north from Scotland between 20:45 and 21:15 UT. This speed was found to be of the order of 202(±27)–236(±32) m s^{-1}, the direction of propagation being toward the west-southwest. Those values suggest the presence of strong westward winds near the dune altitude during the event, possibly generated by the increased geomagnetic activity.

While the present study does not provide definitive answers regarding the nature of the dunes, it brings observational evidence supporting the theory that they are the result of the excitation of oxygen atoms by particle precipitation from the magnetosphere in presence of a mesospheric bore modulating the oxygen density over horizontal scales. For the first time, satellite observations and citizen scientist data were combined to analyze a dune event. Similarly, the first estimations of the phase speed of the dune wavefield provided new elements in the characterization of this recently reported optical phenomenon which could prove crucial to confirm or invalidate the current dune aurora theory in future studies. In a similar manner as for studies of STEVE, the scarcity of suitable geophysical instrumentation at subauroral latitudes makes high-quality citizen scientist observations invaluable to improve the understanding of the complex subauroral lower-thermosphere–ionosphere couplings.

Appendix A: Estimation of Uncertainties in Citizen Scientist Image Analysis

The main source of uncertainties in the dune parameters derived from the analysis of the photographs taken by the citizen scientists is inaccuracies in the mapping of the dune tips to the background nightsky. We present below a simplistic approach to estimate the uncertainties in the derived dune wavelengths and propagation speed.

First of all, one needs to estimate the uncertainties in mapping the dune extremities in terms of azimuth ψ and elevation λ angles in a given photograph. This can only be done empirically by visually determining within which level of accuracy a dune tip can be pinpointed and located in the background nightsky using Stellarium. We evaluate that values of $\delta\psi = \delta\lambda = 0.3°$ are conservative estimates of those pointing inaccuracies.

The resulting uncertainties in the mapping of the dunes at altitude $h = 100$ km above the ground are strongly dependent on the elevation angle λ. It is straightforward to show that, for a given λ, the uncertainty in azimuth $\delta\psi$ results in an uncertainty in the mapping of the point (in the direction perpendicular to the ground projection of the line joining the observer to the dune tip)

$$\delta x = \frac{h}{\sin\lambda}\delta\psi. \tag{A1}$$

Similarly, the uncertainty in elevation $\delta\lambda$ results in an uncertainty in the mapping of the point (in the direction along the ground projection of the line joining the observer to the dune tip)

$$\delta y = \frac{h}{\sin^2\lambda}\delta\lambda. \tag{A2}$$

This leads to an uncertainty in the mapping of a dune tip

$$\delta r(\lambda) = \sqrt{\delta x^2 + \delta y^2} = \frac{h}{\sin^2 \lambda} \sqrt{\sin^2 \lambda (\delta \psi)^2 + (\delta \lambda)^2}. \tag{A3}$$

In practice, the dunes mapped in this study were viewed with elevation angles ranging from 7° to 52°, leading to values of δr ranging from 36 to 1.1 km, respectively. Note that this simplistic reasoning does not take into account uncertainties in the assumed altitude (the triangulation method used in Palmroth, Grandin, Helin, et al., 2020 yielded error bars at about ±3 km for the derived altitude of the dunes) nor in the exact time at which the photographs were taken.

The derivation of the wavelength L of the observed dunes for this study is slightly different from that described in Palmroth, Grandin, Helin, et al. (2020), where the distance between the equatorward tips which were farthest apart from each other was divided by the number of wavelengths between them. Here, we instead calculate the distance between the equatorward dune tip which is the farthest away from the observer and the line defined by the dune finger which is the closest to the observer, and we divide this distance by the number of wavelengths N between the two (see Figure S1 in the Supporting Information for an illustration). This is expected to give more accurate results, especially in cases where the equatorward edge of the dune region is not perpendicular to the dune wave fronts.

The uncertainties in the dune mapping δr are propagated to the wavelength derivations by retaining the mean elevation angle $\bar{\lambda}$ for all the dune tips identified in a given photograph (there are $2N + 2$ dune tips according to the definition of N above) and calculating

$$\delta L = \frac{2\delta r(\bar{\lambda})}{N}. \tag{A4}$$

The uncertainty values for the dune wavelengths given in Section 3.1 are obtained by taking $\bar{\lambda}$ values of 27°, 23°, 9°, and 13° for the dunes observed in Aura, Karmøy, Lendalfoot, and the Isle of Mull, respectively.

Finally, in the derivation of the dune propagation speed u (Section 3.5), we estimate that the beginning and end of the time intervals identified in Figure 6 for the calculation are accurate within $\delta\Delta t = 30$ s. We first calculate the period associated with dune propagation as $T = \Delta t/M$, where M is the number of periods identified during the Δt interval ($M = 8$ or 9 in Section 3.5), and the associated uncertainty is

$$\delta T = \frac{2\delta\Delta t}{M}. \tag{A5}$$

Since the propagation speed is given by $u = L/T$, a simple way to handle uncertainty propagation is to add the relative uncertainties, yielding

$$\frac{\delta u}{u} = \frac{\delta L}{L} + \frac{\delta T}{T}, \tag{A6}$$

which was the formula used to evaluate the uncertainties on the dune propagation speeds.

While not perfect, these estimates nonetheless provide a measure of the uncertainties in the derivation of the dune wavelength and propagation speed as presented in this study.

Conflict of Interest

The authors declare that they have no competing financial interests.

Data Availability Statement

Movie S1 showing a time lapse of the dunes observed from Rattray, Scotland, accompanies this manuscript as Supporting Information. The other photographs by citizen scientists used in the study are those given in Figure 1. The OMNI data can be accessed through the OMNIWeb interface (https://omniweb.gsfc.nasa.gov/).

The SSUSI data are archived at the NASA Space Physics Data Facility (https://spdf.gsfc.nasa.gov/). The SABER data can be obtained from the SABER instrument webpages (http://saber.gats-inc.com/).

Acknowledgments
The authors thank the developers of the Stellarium software (Chéreau, 2020) which was used to retrieve the dune locations based on the photographs. Similarly, they thank Dominic Ford for developing the In-The-Sky.org (https://in-the-sky.org/) website which was used to check the time calibration of the Aura footage. The authors also acknowledge the Finnish aurora enthusiasts' community, especially through the *Revontulikyttääjät* Facebook group and the *Taivaanvahti* service where auroral and astronomical observations are collected and archived (https://www.taivaanvahti.fi/), thanks to whom the dune event was found in the first place. M. Grandin thanks James Russell for valuable feedback on the SABER temperature profile interpretation. M. G. Mlynczak acknowledges support from the NASA Heliophysics Division TIMED Project.
This work was supported by the Academy of Finland through grant number 312351 (FORESAIL) and European Research Council Consolidator Grant 682068-PRESTISSIMO.

References

Archer, W. E., St- Maurice, J. P., Gallardo-Lacourt, B., Perry, G. W., Cully, C. M., Donovan, E., et al. (2019). The vertical distribution of the optical emissions of a steve and picket fence event. *Geophysical Research Letters*, *46*(19), 10719–10725. https://doi.org/10.1029/2019GL084473

Bageston, J. V., Wrasse, C. M., Batista, P. P., Hibbins, R. E., Fritts, D. C., Gobbi, D., & Andrioli, V. F. (2011). Observation of a mesospheric front in a dual duct over King George Island, Antarctica. *Atmospheric Chemistry and Physics Discussions*, *11*(5), 16185–16206. https://doi.org/10.5194/acpd-11-16185-2011

Berger, M. J., Seltzer, S. M., & Maeda, K. (1970). Energy deposition by auroral electrons in the atmosphere. *Journal of Atmospheric and Terrestrial Physics*, *32*, 1015–1045. https://doi.org/10.1016/0021-9169(70)90115-7

Cai, L., Oyama, S., Aikio, A., Vanhamäki, H., & Virtanen, I. (2019). Fabry-Perot interferometer observations of thermospheric horizontal winds during magnetospheric substorms. *Journal of Geophysical Research: Space Physics*, *124*(5), 3709–3728. https://doi.org/10.1029/2018JA026241

Cane, H. V., & Richardson, I. G. (2003). Interplanetary coronal mass ejections in the near-Earth solar wind during 1996-2002. *Journal of Geophysical Research*, *108*(A4), 1156. https://doi.org/10.1029/2002JA009817

Chéreau, F. (2020). *Stellarium. Github repository*. (https://github.com/Stellarium/stellarium, Version 0.20.2, last access: 30.07.2020) Retrieved from https://github.com/Stellarium/stellarium

Davis, T. N., & Sugiura, M. (1966). Auroral electrojet activity indexAEand its universal time variations. *Journal of Geophysical Research*, *71*, 785–801. https://doi.org/10.1029/JZ071i003p00785

Dewan, E. M., & Picard, R. H. (1998). Mesospheric bores. *Journal of Geophysical Research*, *103*(D6), 6295–6305. https://doi.org/10.1029/97JD02498

Dewan, E. M., & Picard, R. H. (2001). On the origin of mesospheric bores. *Journal of Geophysical Research*, *106*(D3), 2921–2927. https://doi.org/10.1029/2000JD900697

Dungey, J. W. (1961). Interplanetary magnetic field and the auroral zones. *Physical Review Letters*, *6*, 47–48. https://doi.org/10.1103/PhysRevLett.6.47

Fechine, J., Wrasse, C. M., Takahashi, H., Medeiros, A. F., Batista, P. P., Clemesha, B. R., et al. (2009). First observation of an undular mesospheric bore in a Doppler duct. *Annales Geophysicae*, *27*(4), 1399–1406. https://doi.org/10.5194/angeo-27-1399-2009

Ferdousi, B., Nishimura, Y., Maruyama, N., & Lyons, L. R. (2019). Subauroral neutral wind driving and its feedback to saps during the 17 march 2013 geomagnetic storm. *Journal of Geophysical Research: Space Physics*, *124*(3), 2323–2337. https://doi.org/10.1029/2018JA026193

Gallardo-Lacourt, B., Liang, J., Nishimura, Y., & Donovan, E. (2018). On the origin of STEVE: Particle precipitation or ionospheric skyglow? *Geophysical Research Letters*, *45*(16), 7968–7973. https://doi.org/10.1029/2018GL078509

García-Comas, M., López-Puertas, M., Marshall, B. T., Wintersteiner, P. P., Funke, B., Bermejo-Pantaleón, D., et al. (2008). Errors in Sounding of the Atmosphere using Broadband Emission Radiometry (SABER) kinetic temperature caused by non-local-thermodynamic-equilibrium model parameters. *Journal of Geophysical Research*, *113*(D24), D24106. https://doi.org/10.1029/2008JD010105

Gillies, D. M., Donovan, E., Hampton, D., Liang, J., Connors, M., Nishimura, Y., et al. (2019). First observations from the TREx spectrograph: The optical spectrum of STEVE and the picket fence phenomena. *Geophysical Research Letters*, *46*(13), 7207–7213. https://doi.org/10.1029/2019GL083272

Grandin, M. (2020). Small-scale optical atmospheric emissions discovered using citizen science photography. *AGU Advances*, *1*(4), e2020AV000268. https://doi.org/10.1029/2020AV000268

Harding, B. J., Mende, S. B., Triplett, C. C., & Wu, Y. J. J. (2020). A mechanism for the STEVE continuum emission. *Geophysical Research Letters*, *47*(7), e87102. https://doi.org/10.1029/2020GL087102

Hauchecorne, A., Chanin, M. L., & Wilson, R. (1987). Mesospheric temperature inversion and gravity wave breaking. *Geophysical Research Letters*, *14*(9), 933–936. https://doi.org/10.1029/GL014i009p00933

Hecht, J. H., Christensen, A. B., Strickland, D. J., & Meier, R. R. (1989). Deducing composition and incident electron spectra from ground-based auroral optical measurements: Variations in oxygen density. *Journal of Geophysical Research*, *94*(A10), 13553–13563. https://doi.org/10.1029/JA094iA10p13553

Hecht, J. H., Strickland, D. J., Christensen, A. B., Kayser, D. C., & Walterscheid, R. L. (1991). Lower thermospheric composition changes derived from optical and radar data taken at Sondre Stromfjord during the great magnetic storm of February 1986. *Journal of Geophysical Research*, *96*(A4), 5757–5776. https://doi.org/10.1029/90JA02460

Heelis, R. A., & Maute, A. (2020). Challenges to understanding the earth's ionosphere and thermosphere. *Journal of Geophysical Research: Space Physics*, *125*(7), e27497. https://doi.org/10.1029/2019JA027497

Hozumi, Y., Saito, A., Sakanoi, T., Yamazaki, A., & Hosokawa, K. (2018). Mesospheric bores at southern midlatitudes observed by ISS-IMAP/VISI: A first report of an undulating wave front. *Atmospheric Chemistry and Physics*, *18*(22), 16399–16407. https://doi.org/10.5194/acp-18-16399-2018

Hozumi, Y., Saito, A., Sakanoi, T., Yamazaki, A., Hosokawa, K., & Nakamura, T. (2019). Geographical and seasonal variability of mesospheric bores observed from the International Space Station. *Journal of Geophysical Research: Space Physics*, *124*(5), 3775–3785. https://doi.org/10.1029/2019JA026635

Hundhausen, A. J., Bame, S. J., Asbridge, J. R., & Sydoriak, S. J. (1970). Solar wind proton properties: Vela 3 observations from July 1965 to June 1967. *Journal of Geophysical Research*, *75*(25), 4643–4657. https://doi.org/10.1029/JA075i025p04643

Ishii, M., Oyama, S., Nozawa, S., Fujii, R., Sagawa, E., Watari, S., & Shinagawa, H. (1999). Dynamics of Neutral Wind in the polar region observed with two Fabry-Perot Interferometers. *Earth Planet Sp*, *51*, 833–844. https://doi.org/10.1186/BF03353242

Iyemori, T. (1990). Storm-time magnetospheric currents inferred from mid-latitude geomagnetic field variations. *Journal of Geomagnetism and Geoelectricity*, *42*(11), 1249–1265. https://doi.org/10.5636/jgg.42.1249

King, J. H., & Papitashvili, N. E. (2005). Solar wind spatial scales in and comparisons of hourly Wind and ACE plasma and magnetic field data. *Journal of Geophysical Research*, *110*, 2104. https://doi.org/10.1029/2004JA010649

Laughman, B., Fritts, D. C., & Werne, J. (2009). Numerical simulation of bore generation and morphology in thermal and Doppler ducts. *Annales Geophysicae*, *27*(2), 511–523. https://doi.org/10.5194/angeo-27-511-2009

Lee, C. N., Min, K. W., Lee, J.-J., Parks, G. K., Fillingim, M. O., Lummerzheim, D., et al. (2010). Spectral observations of FUV auroral arcs and comparison with inverted-V precipitating electrons. *Journal of Geophysical Research*, *115*(A9), A09223. https://doi.org/10.1029/2009JA015071

Li, Q., Xu, J., Yue, J., Liu, X., & Yuan, W. (2019). Evolution of a mesospheric bore in a duct observed by ground-based double-layer imagers and satellite observations over the Tibetan plateau region. *Journal of Geophysical Research: Space Physics*, *124*(2), 1377–1388. https://doi.org/10.1029/2018JA026125

Lukianova, R., Kozlovsky, A., & Lester, M. (2018). Climatology and inter-annual variability of the polar mesospheric winds inferred from meteor radar observations over Sodankylä (67N, 26E) during solar cycle 24. *Journal of Atmospheric and Solar-Terrestrial Physics*, *171*, 241–249. https://doi.org/10.1016/j.jastp.2017.06.005

MacDonald, E. A., Donovan, E., Nishimura, Y., Case, N. A., Gillies, D. M., Gallardo-Lacourt, B., et al. (2018). New science in plain sight: Citizen scientists lead to the discovery of optical structure in the upper atmosphere. *Science Advances*, *4*(3), eaaq0030. https://doi.org/10.1126/sciadv.aaq0030

Mende, S. B., Harding, B. J., & Turner, C. (2019). Subauroral green STEVE arcs: Evidence for low-energy excitation. *Geophysical Research Letters*, *46*(24), 14256–14262. https://doi.org/10.1029/2019GL086145

Miller, S. D., Mills, S. P., Elvidge, C. D., Lindsey, D. T., Lee, T. F., & Hawkins, J. D. (2012). Suomi satellite brings to light a unique Frontier of nighttime environmental sensing capabilities. *Proceedings of the National Academy of Sciences*, *109*(39), 15706–15711. https://doi.org/10.1073/pnas.1207034109

Miller, S. D., Straka, W. C., Yue, J., Smith, S. M., Alexander, M. J., Hoffmann, L., Setvák, M., et al. (2015). Upper atmospheric gravity wave details revealed in nightglow satellite imagery. *Proceedings of the National Academy of Sciences of the United States of America*, *112*(49), E6728–E6735. https://doi.org/10.1073/pnas.1508084112

Miller, S., Straka, W., Mills, S., Elvidge, C., Lee, T., Solbrig, J., et al. (2013). Illuminating the capabilities of the suomi national polar-orbiting partnership (NPP) visible infrared imaging radiometer suite (VIIRS) day/night band. *Remote Sensing*, *5*(12), 6717–6766. https://doi.org/10.3390/rs5126717

Nygrén, T., Aikio, A. T., Voiculescu, M., & Cai, L. (2015). Radar observations of simultaneous traveling ionospheric disturbances and atmospheric gravity waves. *Journal of Geophysical Research: Space Physics*, *120*(5), 3949–3960. https://doi.org/10.1002/2014JA020794

Palmroth, M., Grandin, M., Helin, M., Koski, P., Oksanen, A., Glad, M. A., et al. (2020). Citizen scientists discover a new auroral form: Dunes provide insight into the upper atmosphere. *AGU Advances*, *1*(1), e2019AV000133. https://doi.org/10.1029/2019AV000133

Palmroth, M., Grandin, M., Sarris, T., Doornbos, E., Tourgaidis, S., Aikio, A., et al. (2021). Lower-thermosphere–ionosphere (LTI) quantities: current status of measuring techniques and models. *Annales Geophysicae*, *39*, 189–237. https://doi.org/10.5194/angeo-39-189-2021

Paxton, L. J., Meng, C.-I., Fountain, G. H., Ogorzalek, B. S., Darlington, E. H., Gary, S. A., et al. (1993). SSUSI - Horizon-to-horizon and limb-viewing spectrographic imager for remote sensing of environmental parameters. In R. E. Huffman (Ed.), *Ultraviolet technology IV* (Vol. 1764, pp. 161–176). https://doi.org/10.1117/12.140846

Paxton, L. J., Morrison, D., Zhang, Y., Kil, H., Wolven, B., Ogorzalek, B. S., et al. (2002). Validation of remote sensing products produced by the Special Sensor Ultraviolet Scanning Imager (SSUSI): A far UV-imaging spectrograph on DMSP F-16. In A. M. Larar & M. G. Mlynczak (Eds.), *Optical Spectroscopic Techniques, Remote Sensing, and Instrumentation for Atmospheric and Space Research IV* (Vol. 4485, pp. 338–348). https://doi.org/10.1117/12.454268

Paxton, L. J., Schaefer, R. K., Zhang, Y., & Kil, H. (2017). Far ultraviolet instrument technology. *Journal of Geophysical Research: Space Physics*, *122*(2), 2706–2733. https://doi.org/10.1002/2016JA023578

Richardson, I. G., & Cane, H. V. (2010). Near-earth interplanetary coronal mass ejections during solar cycle 23 (1996–2009): Catalog and summary of properties. *Solar Physics*, *264*(1), 189–237. https://doi.org/10.1007/s11207-010-9568-6

Richardson, I. G., & Cane, H. V. (2012). Near-earth solar wind flows and related geomagnetic activity during more than four solar cycles (1963–2011). *Journal of Space Weather and Space Climate*, *2*, A02. https://doi.org/10.1051/swsc/2012003

Roldugin, V., Cherniakov, S., & Roldugin, A. (2016). Simultaneous observations of gravity waves in auroras and partial reflection radar data. In 41st COSPAR scientific assembly (41). C2.1-11-16.

Russell, J. M., Mlynczak, M. G., Gordley, L. L., Tansock, J. J., & Esplin, R. W. (1999). Overview of the SABER experiment and preliminary calibration results. In A. M. Larar (Ed.), *Optical spectroscopic techniques and instrumentation for atmospheric and space research III* (Vol. 3756, pp. 277–288). https://doi.org/10.1117/12.366382

Sarris, T. E. (2019). Understanding the ionosphere thermosphere response to solar and magnetospheric drivers: Status, challenges and open issues. *Philosophical Transactions of the Royal Society A*, *377*(2148), 20180101. https://doi.org/10.1098/rsta.2018.0101

Seaman, C. J., & Miller, S. D. (2013). VIIRS captures aurora motions. *Bulletin of the American Meteorological Society*, *94*(10), 1491–1493. https://doi.org/10.1175/BAMS-D-12-00221.1

Semeter, J., Hunnekuhl, M., MacDonald, E., Hirsch, M., Zeller, N., Chernenkoff, A., & Wang, J. (2020). The mysterious green streaks below steve. *AGU Advances*, *1*(4), e2020AV000183. https://doi.org/10.1029/2020AV000183

Seyler, C. E. (2005). Internal waves and undular bores in mesospheric inversion layers. *Journal of Geophysical Research*, *110*(D9), D09S05. https://doi.org/10.1029/2004JD004685

She, C. Y., Li, T., Williams, B. P., Yuan, T., & Picard, R. H. (2004). Concurrent OH imager and sodium temperature/wind lidar observation of a mesopause region undular bore event over Fort Collins/Platteville, Colorado. *Journal of Geophysical Research*, *109*(D22), D22107. https://doi.org/10.1029/2004JD004742

Smith, S. M., Stober, G., Jacobi, C., Chau, J. L., Gerding, M., Mlynczak, M. G., et al. (2017). Characterization of a double mesospheric bore over Europe. *Journal of Geophysical Research: Space Physics*, *122*(9), 9738–9750. https://doi.org/10.1002/2017JA024225

Smith, S. M., Taylor, M. J., Swenson, G. R., She, C.-Y., Hocking, W., Baumgardner, J., & Mendillo, M. (2003). A multidiagnostic investigation of the mesospheric bore phenomenon. *Journal of Geophysical Research*, *108*(A2), 1083. https://doi.org/10.1029/2002JA009500

Strickland, D. J., Meier, R. R., Hecht, J. H., & Christensen, A. B. (1989). Deducing composition and incident electron spectra from ground-based auroral optical measurements: Theory and model results. *Journal of Geophysical Research*, *94*(A10), 13527–13539. https://doi.org/10.1029/JA094iA10p13527

Su, Y., Yue, J., Liu, X., Miller, S. D., III, W. C. S., III, Smith, S. M., et al. (2018). Mesospheric bore observations using suomi-NPP VIIRS DNB during 2013–2017. *Remote Sensing*, *10*(12), 1935. https://doi.org/10.3390/rs10121935

Wang, H., Lühr, H., & Ma, S. Y. (2012). The relation between subauroral polarization streams, westward ion fluxes, and zonal wind: Seasonal and hemispheric variations. *Journal of Geophysical Research*, *117*(A4), A04323. https://doi.org/10.1029/2011JA017378

Wilson, III, L. B., III, Stevens, M. L., Kasper, J. C., Klein, K. G., Maruca, B. A., Bale, S. D., et al. (2018). The statistical properties of solar wind temperature parameters near 1 au. *Asia Pacific Journal of Social Work*, *236*(2), 41. https://doi.org/10.3847/1538-4365/aab71c

Yuan, T., Pautet, P.-D., Zhao, Y., Cai, X., Criddle, N. R., Taylor, M. J., & Pendleton, W. R. (2014). Coordinated investigation of midlatitude upper mesospheric temperature inversion layers and the associated gravity wave forcing by Na lidar and Advanced Mesospheric Temperature Mapper in Logan, Utah. *Journal of Geophysical Research: Atmospheres*, *119*(7), 3756–3769. https://doi.org/10.1002/2013JD020586

Yue, J., & Lyons, W. A. (2015). Structured elves: Modulation by convectively generated gravity waves. *Geophysical Research Letters*, *42*(4), 1004–1011. https://doi.org/10.1002/2014GL062612

Yue, J., She, C.-Y., Nakamura, T., Harrell, S., & Yuan, T. (2010). Mesospheric bore formation from large-scale gravity wave perturbations observed by collocated all-sky OH imager and sodium lidar. *Journal of Atmospheric and Solar-Terrestrial Physics*, *72*(1), 7–18. https://doi.org/10.1016/j.jastp.2009.10.002